Chapter 4

Fiber-Random Amplifying Medium : An optical realization of the Arrhenius cascade

4.1 Motivation

In the previous chapters, we had shown Lévy statistical fluctuations in the emission intensity from dye-scatterer random amplifying media (RAMs). The large jumps in intensity resulted from rare events where a photon traversed a long path in the gain medium owing to multiple scattering and was significantly amplified. The work presented in this chapter was undertaken to establish the crucial role of the rare long amplifying paths in causing Lévy fluctuations in a RAM. To this end, we devise a novel specially structured system, the F-RAM (Fiber-Random Amplifying Medium), which is an aggregate of segments of active fiber embedded randomly in a passive scattering bulk. This tailored system permits intentional introduction of long amplifying paths with desired probability of occurrence. The mean length of the fiber segments was much greater than the mean free path of light in the passive scattering background, making the probability of prompt escape from the sample much higher. Thus, the long amplifying photon paths in the F-RAM are even rarer than those in a RAM. The high gain in the fiber, however, makes it possible to observe these very

rare events as random large jumps in the emission intensity as the photons on entering such long though exponentially rare paths undergo exponentially high amplification.

In the context of Lévy statistics, the theoretical Arrhenius cascade model is often employed. This model is described in the next section (4.2). We realize a practical analogy in optics by devising the F-RAM, which is described in section 4.3. We, then extend our theoretical analysis for the RAM (discussed in chapter 2, section 2.2) to the case of an F-RAM in section 4.4, followed by experiments described in section 4.5. Section 4.6 discusses the salient results of the experiments. Section 4.7 draws the comparison between a RAM and an F-RAM. The chapter ends in section 4.8 which gives the conclusions of our work.

4.2   Arrhenius Cascade

The Arrhenius cascade [1] consists of a tilted washboard which has n local potential minima or wells, labelled by i, separated from the next potential minimum $i + 1$ by a potential hill (Fig. 4.1). The depths of the local minima are random, and follow the probability density $p(U_i)$ for the well depth (U_i) (Fig. 4.2(a): dotted curve), given as,

$$p(U_i) = \frac{1}{U_o}\, e^{-(U_i/U_o)}, \tag{4.1}$$

where, U_o is the mean well depth.

At any time, the physical system is trapped in one of the local potential wells. The global tilt of the potential hill is large enough to prevent the particle from performing upward jumps. Thus, the particle can only cascade downwards. The particle spends a time t_i in the ith potential well, the time being dependent exponentially on the depth of the well (Fig. 4.2(a): solid curve). The activated trapping time (t_i) in the ith well is,

$$t_i = t_o\, e^{(U_i/kT)} \equiv t_i(U_i), \tag{4.2}$$

where, t_o is characteristic time, K is the Boltzmann constant, and T is the temperature. Thus, though deep wells are exponentially improbable, their presence increases the residence time exponentially. The model examines the total time taken by a particle to descend the washboard. Thermal fluctuations make the particle perform sudden downward jumps from one
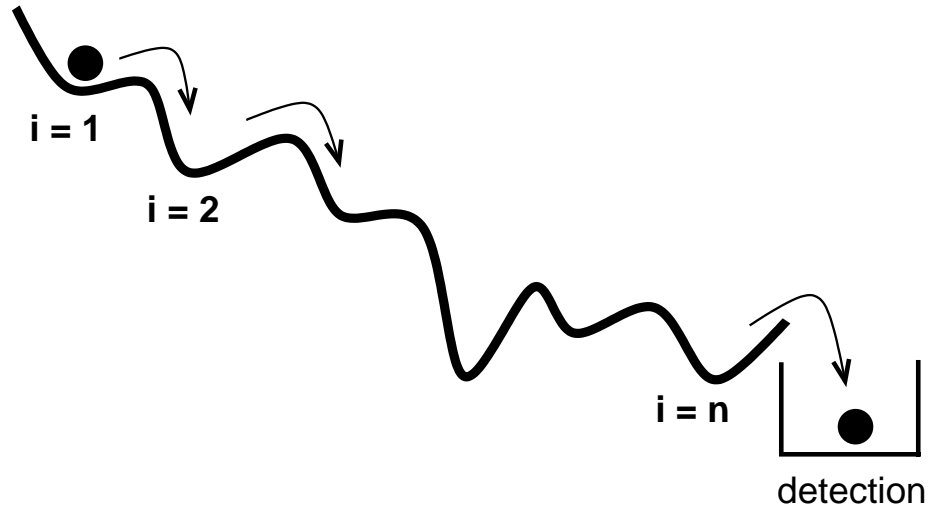
Figure 4.1: *Schematic of Arrhenius cascade model showing a particle descending an incline with potential wells of random depths.*

well to the other one. The total time of descent is $t = \sum_{1=1}^{n} t_i$.

Since, $t_i \equiv t_i(U_i)$, by the law of probability,

$$
\begin{aligned}
p(t_i) \, dt_i &= p(U_i) \, dU_i \\
\Rightarrow \qquad p(t_i) &= p(U_i) \, \frac{dU_i}{dt_i} \\
&= \frac{1}{U_o} \, e^{-(U_i/U_o)} \, \frac{KT}{t_i}
\end{aligned}
\qquad (4.3)
$$

(using Eqs (4.1) and (4.2)).

From Eq (4.2), we get

$$
\begin{aligned}
e^{U_i/KT} &= \frac{t_i}{t_o} \\
\Rightarrow \qquad U_i &= KT \, ln\!\left(\frac{t_i}{t_o}\right) \\
\Rightarrow \qquad \frac{-U_i}{U_o} &= \frac{-KT}{U_o} \, ln\!\left(\frac{t_i}{t_o}\right) = ln\!\left(\frac{t_i}{t_o}\right)^{-(KT/U_o)} \\
\Rightarrow \qquad e^{-(U_i/U_o)} &= e^{\,ln(t_i/t_o)^{-\alpha}} = \left(\frac{t_i}{t_o}\right)^{-\alpha}, \qquad : (using, \; e^{lnx} = x) \quad (4.4)
\end{aligned}
$$

where, $\alpha = KT/U_o$

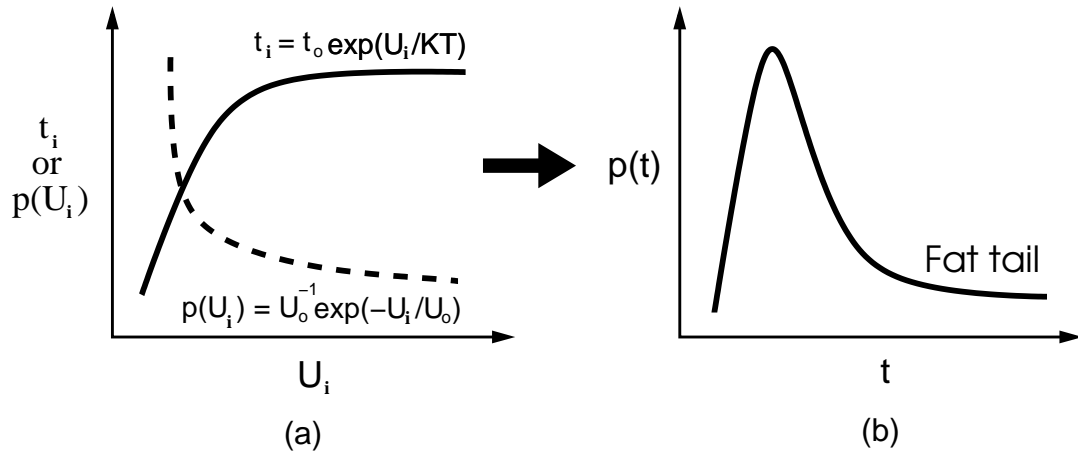Substituting Eq (4.4) in Eq (4.3), yields an inverse power law probability density for the

Figure 4.2: *(a) Residence time (t_i) of particle in a well of depth U_i (bold curve) and probability density ($p(U_i)$) for well depth (dashed curve), (b) Probability density of total time of descent of the particle.*

trapping time,

$$p(t_i) \;=\; \alpha \, \frac{t_o^{\alpha}}{t_i^{1+\alpha}} \;\approx\; t_i^{-(1+\alpha)} \qquad : \;\; \alpha = \frac{KT}{U_o} \qquad (4.5)$$

For $\alpha \geq 2$, corresponding to high temperature (T) the particle has a fast descent and the second moment is finite. The corresponding total-time ($t/\sqrt{n}$) probability density tends to the Gaussian limit – the classical Central Limit Theorem – as $n \rightarrow \infty$. For $0 < \alpha < 2$ (corresponding to intermediate or low temperatures), however, the second moment of the individual trapping time diverges, and the corresponding total-time ($t/n^{1/\alpha}$) tends to the Lévy distribution (Fig. 4.2(b)) with an inverse power law probability density $\sim t^{-(1+\alpha)}$ asymptotically (the Generalized Central Limit Theorem, α being the Lévy exponent). In particular, while for $1 \leq \alpha < 2$ (intermediate temperature regime) the distribution has finite mean but infinite variance, for $0 < \alpha < 1$ (low temperature regime), both the mean and the variance are divergent. Thus, we have the Gaussian statistics at high temperatures and the Lévy statistics at low and intermediate temperatures for the cascade.

In the following section we show how the F-RAM, devised by us, simulates physically an Arrhenius cascade.

4.3   Fiber-Random Amplifying Medium (F-RAM)

The F-RAM is an aggregation of segments of dye-doped amplifying (one-dimensional) fibers (Bicron, fluorescent red) embedded randomly in a passive medium of granular starch (Fig. 4.3). These plastic fibers fluoresce in the orange-red when pumped by green light that can enter the fibers through their cylindrical surfaces anywhere along their lengths. The emitted light (fluorescence) is, however, guided mainly along the length of the fiber, and it emerges from either end amplified by a factor that increases exponentially with its path-length l in the fiber ($g(l) = exp(l/l_g)$). It may be noted that in an F-RAM, the random aggregation of the amplifying fibers itself provides some scattering, which is enhanced by the addition of passive point-like scatterers e.g., polystyrene microspheres or granular starch. Thus, in an F-RAM, light propagation proceeds by diffusion due to random scattering in the passive bulk and waveguidance through the randomly embedded active fiber segments. Such a partially structured disorder is expected to enhance the Lévy fluctuations. Further, in contrast to an ordinary optical fiber that merely guides the light incident at one of its ends to the other end (Fig. 4.4(a)), an active fiber is a dye-doped optical fiber, that amplifies the light (via stimulated emission) as it propagates through its length with the amplification proportional to the active fiber length (Fig. 4.4(b)).

To exploit the fact that two functions, one exponentially increasing and the other exponentially falling, can combine to give rise to Gaussian or Lévy statistics depending on the relative values of the two exponents as discussed in the previous section, we tailored our F-RAM system, such that the lengths of the fiber segments follow an exponential probability density :

$$p(l) = \frac{1}{l_a} \, e^{-(l/l_a)}, \tag{4.6}$$

where, l_a is the mean length of the fiber. The F-RAM, thus, predominantly consists of short active fiber pieces while the long active fibers are exponentially rare. On entering an active fiber, a photon must travel its entire length thereby acquiring gain which increases exponentially with the fiber length.

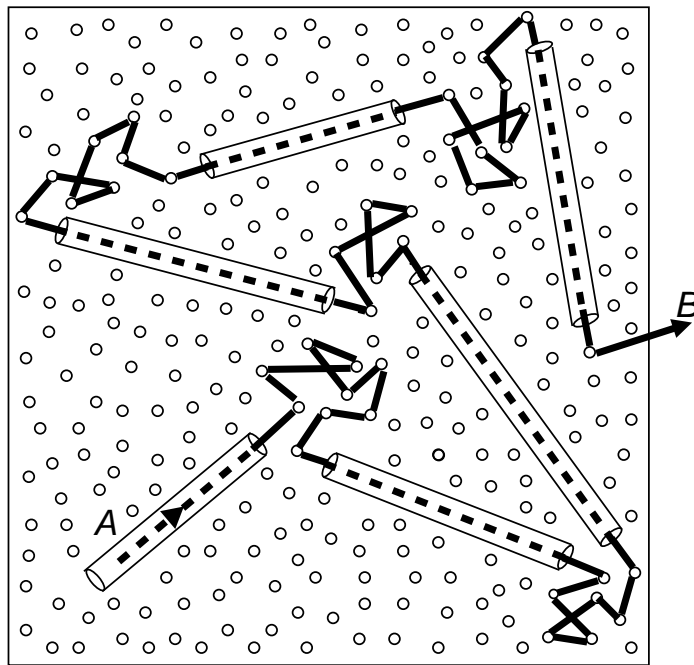$$g \;=\; \frac{I(l)}{I_o} \;=\; e^{(l/l_g)} \equiv g(l) \tag{4.7}$$

Figure 4.3: *Schematic of the F-RAM : In a typical photon path (A → B), photons are am-plified along dashed paths (within the active fibers), and are multiply scattered along solid lines in between transit through segments of fibers.*
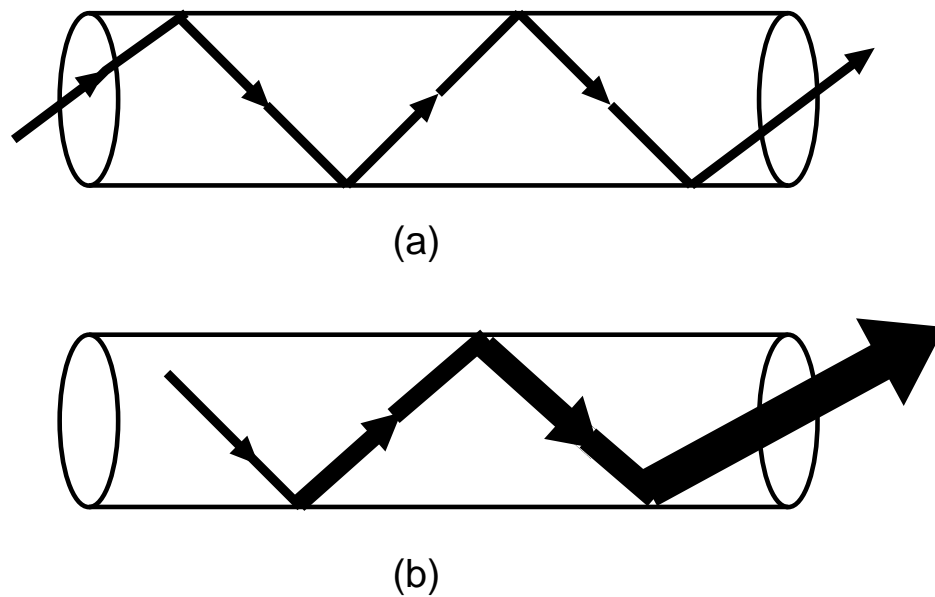

(a)

(b)

Figure 4.4: *Ordinary (non-amplifying) optical fiber vs dye-doped (amplifying) fiber.*

where, l is length of the single active fiber, l_g is the gain length of the active fiber, $I(l)$ is the intensity after traversing the distance l and I_o is the incident intensity.

Thus, long fibers, though exponentially rare, provide exponentially high gain.

Since, $g \equiv g(l)$, by the law of probability, the probability distribution of the total gain $p(g)$ acquired by the photon before exiting the medium,

$$
\begin{aligned}
p(g)\, dg &= p(l)\, dl \\
\Rightarrow \qquad p(g) &= p(l)\, \frac{dl}{dg} \\
&= \frac{1}{l_a}\, e^{-(l/l_a)}\, \frac{l_g}{g}
\end{aligned}
\tag{4.8}
$$

(using Eqs (4.6) and (4.7)).

From Eq (4.7), we get

$$
\begin{aligned}
l &= l_g\, lng \\
\Rightarrow \qquad \frac{-l}{l_a} &= \frac{-l_g}{l_a}\, lng = ln(g)^{-(l_g/l_a)} \\
\Rightarrow \qquad e^{-(l/l_a)} &= e^{\,ln(g)^{-\alpha}} = g^{-\alpha},
\end{aligned}
\tag{4.9}
$$

where, $\alpha = l_g/l_a$.

Substituting Eq (4.9) in Eq (4.8), gives and inverse power law function for the total gain

$$
p(g) = \frac{\alpha}{g^{1+\alpha}} \approx g^{-(1+\alpha)} \qquad : \alpha = \frac{l_g}{l_a}
\tag{4.10}
$$

Thus, while for $\alpha \geq 2$ Gaussian distribution is expected, for $0 < \alpha < 2$, Lévy distribution will be obtained. This suggests that the Lévy exponent may be tuned by altering the gain or the length distribution of the fiber. Clearly, in an F-RAM, l_a and l_g are analogous to U_o and T respectively, of the Arrhenius cascade.

Next, we discuss the generalization of our theoretical analysis for a RAM to an F-RAM.

4.4 Theoretical analysis

In chapter 2 (section 2.2), we had shown from theoretical considerations that for a diffusive dye-scatterer RAM composed of point-like scatterers randomly dispersed in an amplifying

continuum, the probability density for the total gain ($p_g(g)$) acquired by a spontaneously emitted diffusively propagating photon as a result of multiple scattering within the amplifying medium is given as

$$p_g(g) = \sum_{m=1}^{\infty} \left(\frac{8\pi a\rho_o l_t l_g}{3} \right) \frac{1}{g^{1+\alpha_m}}, \tag{4.11}$$

where, $\alpha_m = m^2(\pi^2 l_t l_g/3a^2) \equiv m^{th}$ Lévy exponent.

We first generalize the analytic treatment of the conventional RAM for an F-RAM through an effective-medium theory. Here, the F-RAM is considered as a composite medium with a volume-fraction v_a of the active medium embedded in a passive, diffusive medium of volume-fraction v_p with the transport mean free path l_p. The amplifying medium is a random aggregate of active fiber pieces of radius a and mean length l_a (mean volume $\pi a^2 l_a$). As the fiber provides waveguidance over its length (few millimeters), which is much greater than the transport mean free path in the passive bulk (few micrometers), the direction of propagation of a photon, upon exiting a fiber is rapidly randomized. Thus, the mean free path of the photons in the *active* medium is l_a itself. We now combine these two random components into the simplest effective-medium using the Matthiessen rule [2]. Thus, the photons diffuse within the F-RAM while following the diffusion equation :

$$\frac{\partial \rho(\vec{\mathbf{r}}, t)}{\partial t} = D \, \nabla^2 \rho(\vec{\mathbf{r}}, t) \tag{4.12}$$

where, $D = cl_{eff}/3$ is the diffusion constant, and $1/l_{eff} = v_a/l_a + v_p/l_p$. These diffusively propagating photons undergo amplification $g = e^{v_a ct/l_g}$ in time t. Proceeding as in chapter 2 (section 2.2), we obtain the rate of emission as :

$$p_I(t) = \sum_{m=1}^{\infty} (8\pi a\rho_o D) \, e^{-(m\pi/a)^2 \, tD} \tag{4.13}$$

Now, the intensity gain in the F-RAM is given as :

$$g = e^{cv_a t/l_g} \tag{4.14}$$

$$\Rightarrow g \equiv g(t) \tag{4.15}$$

From the law of probabilities, we get

$$p_g(g) \, dg = p_I(t) \, dt$$

$$\Rightarrow \quad p_g(g) = p_I(t) \, \frac{dt}{dg} \tag{4.16}$$

Using Eqs (4.13), (4.14) and (4.16), we get

$$p_g(g) = \sum_{m=1}^{\infty} (8\pi a \rho_o D) \frac{l_g}{c v_a g} e^{-(m\pi/a)^2 D l_g \ln g/c v_a} \tag{4.17}$$

Thus,

$$p_g(g) = \sum_{m=1}^{\infty} (8\pi a \rho_o D) \frac{l_g}{c v_a g} e^{\ln (g)^{-\alpha_m}} = \sum_{m=1}^{\infty} (8\pi a \rho_o D) \frac{l_g}{c v_a g} g^{-\alpha_m}, \tag{4.18}$$

where, $\alpha_m = (m\pi/a)^2 (Dl_g/c v_a) = m^2(\pi^2 l_{eff} l_g/3a^2 v_a) = m^2[\pi^2 l_g l_a l_p/3a^2 v_a(v_a l_p + v_p l_a)]$ (using, $D = c l_{eff}/3$ and $e^{\ln (g)^{-\alpha_m}} = g^{-\alpha_m}$)

Thus, the probability distribution for the gain $p_g(g)$ is obtained as

$$p_g(g) = \sum_{m=1}^{\infty} \left(\frac{8\pi a \rho_o D l_g}{c v_a} \right) \frac{1}{g^{1+\alpha_m}} \equiv \sum_{m=1}^{\infty} \left(\frac{8\pi a \rho_o l_{eff} l_g}{3 v_a} \right) \frac{1}{g^{1+\alpha_m}} \tag{4.19}$$

where, $\alpha_m = m^2(\pi^2 l_{eff} l_g/3a^2 v_a) \equiv$ the mth Lévy exponent.

As was argued in section 2.2 of chapter 2, it suffices to consider only the smallest Lévy exponent (α_1). Eq (4.19) suggests a Lévy-like fat tail for $\alpha_1 < 2$ and a finite second moment akin to Gaussian behaviour for $\alpha_1 \geq 2$. The Lévy exponent is now tunable by gain and also by l_{eff}, which depends on l_a, l_p, v_a and v_p. These features are confirmed through our experiments discussed below.

4.5 Experimental Details

Experiments were conducted on tailored F-RAMs with N ($N = 500$) segments of amplifying fibers embedded randomly in passive scattering medium provided by suspension of polystyrene microspheres in water (BangsLabs, size = 0.13 μm) or granular starch ($\sim$ 1 mm^3). The scatterers had negligible absorption at the wavelengths of interest and were added to provide the random passive scattering background. In all these systems, the lengths (l) of the amplifying fibers ranged from 1 mm to 20 mm and followed an exponential distribution $p(l)$ (Eq 4.6) with $l_a = 5$ mm (Fig. 4.5). The F-RAM contained in a glass cuvette of size 3 cm $\times$ 3 cm $\times$ 6 cm was pumped optically by 10 ns pulses (10 Hz repetition rate) at 532 nm
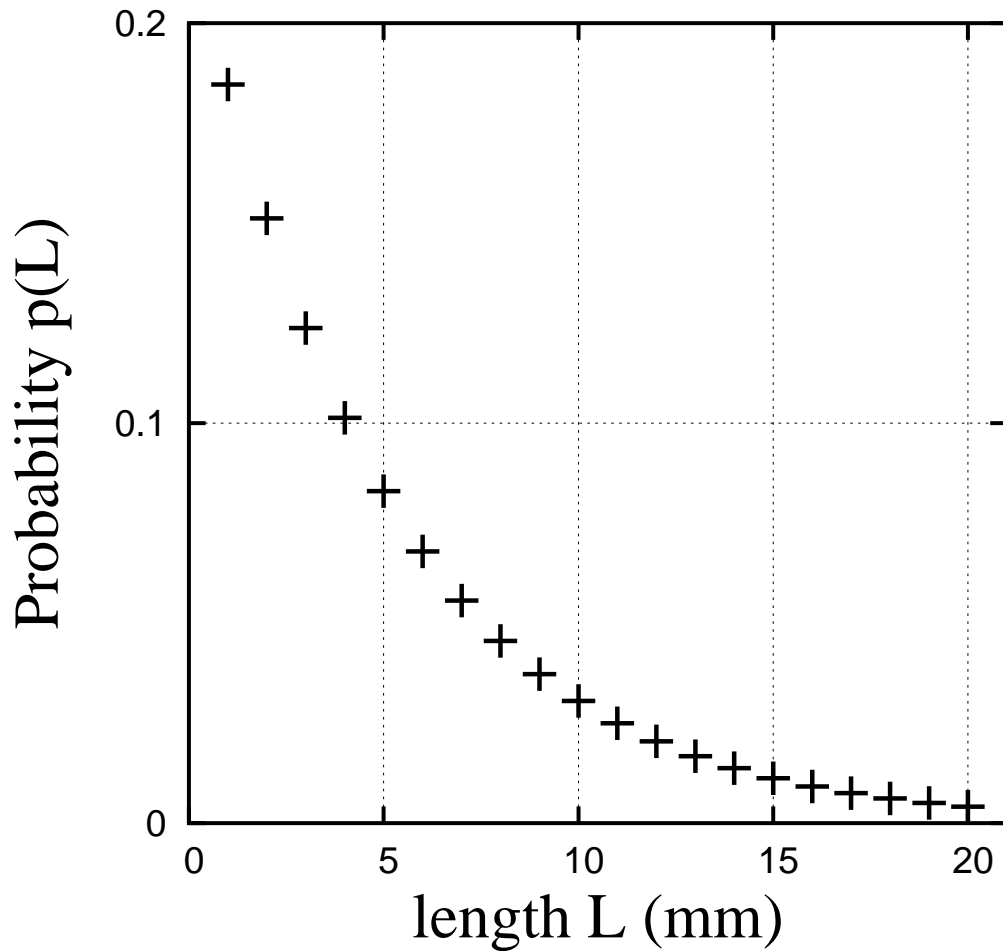
Figure 4.5: *Probability distribution of the fiber lengths (N=500). It shows that while the probability to find short active fibers is large, the probability to find long active fibers is exponentially small.*

from a frequency doubled Nd:YAG laser (Fig. 4.6). The incident pulse was split into two by a beamsplitter (R/T = 50/50). While the transmitted beam was incident on the sample, the reflected part was used to monitor the energy of the pump pulse by the energy meter (Laser Probe Inc., Rj-7620). The pump energy was maintained constant throughout an experimental run. The emission (fluorescence) from the system was collected, by an ordinary optical fiber, in a direction transverse to the pump beam, and the spectrum recorded with a PC-based fiber-optic spectrometer (Ocean-Optics S2000).
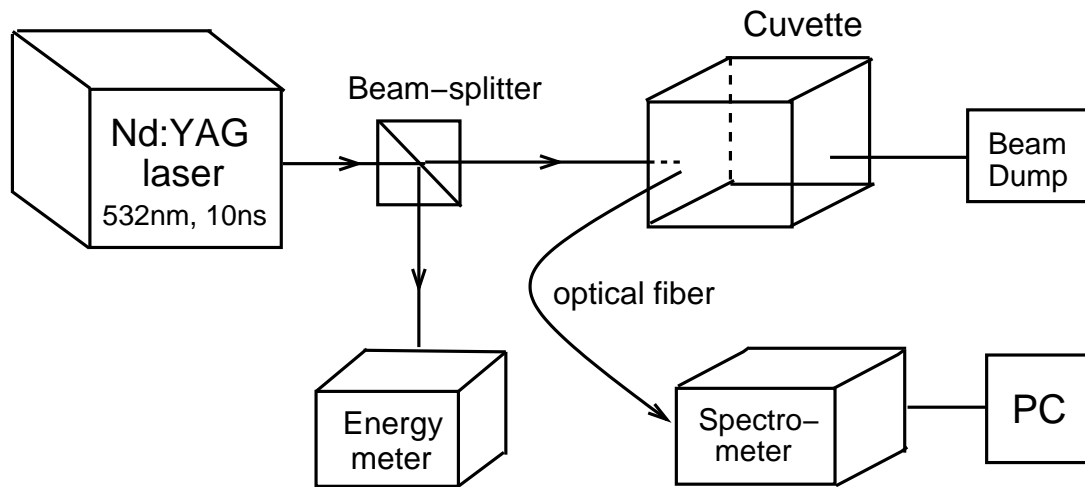
Figure 4.6: *Schematic of the experimental set-up*

4.6   Results

Gain narrowing

The F-RAM was first checked for gain-narrowing. In particular, its emission spectra (for a given macroscopic complexion) as function of pump energy were recorded. Figures 4.7(a)-(d) show the spectra as function of pump energy for N=500 F-RAM in passive scattering medium of polystyrene microspheres or water. Each figure contains four typical emission spectra (A-D) at increasing pumping. The F-RAM showed broad emission (width ~30 nm) typical of dyes at low pump energies (~ 2 mJ), and exhibited gain narrowing (width < 5 nm) with the intensity peaking at ~640 nm at above threshold (3-5 mJ).

We then studied another system that was a collection of millimeter (~ 2-3 mm) sized pieces of active fiber embedded in passive scattering medium of polystyrene microspheres or water as function of pump energy (Figs 4.8(a)-(d)). It is worth noting here that unlike the N=500 F-RAM where the lengths of the fiber segments follow an exponential probability density (Eq 4.6), the collection of millimeter (~ 2-3 mm) sized pieces of active fiber are all of the same lengths. This study was undertaken to examine the effect of the length of active fibers on their emission spectra. Each figure contains four emission spectra (A-D), corresponding to increasing pump energies. The emission spectra (A) recorded at the lowest
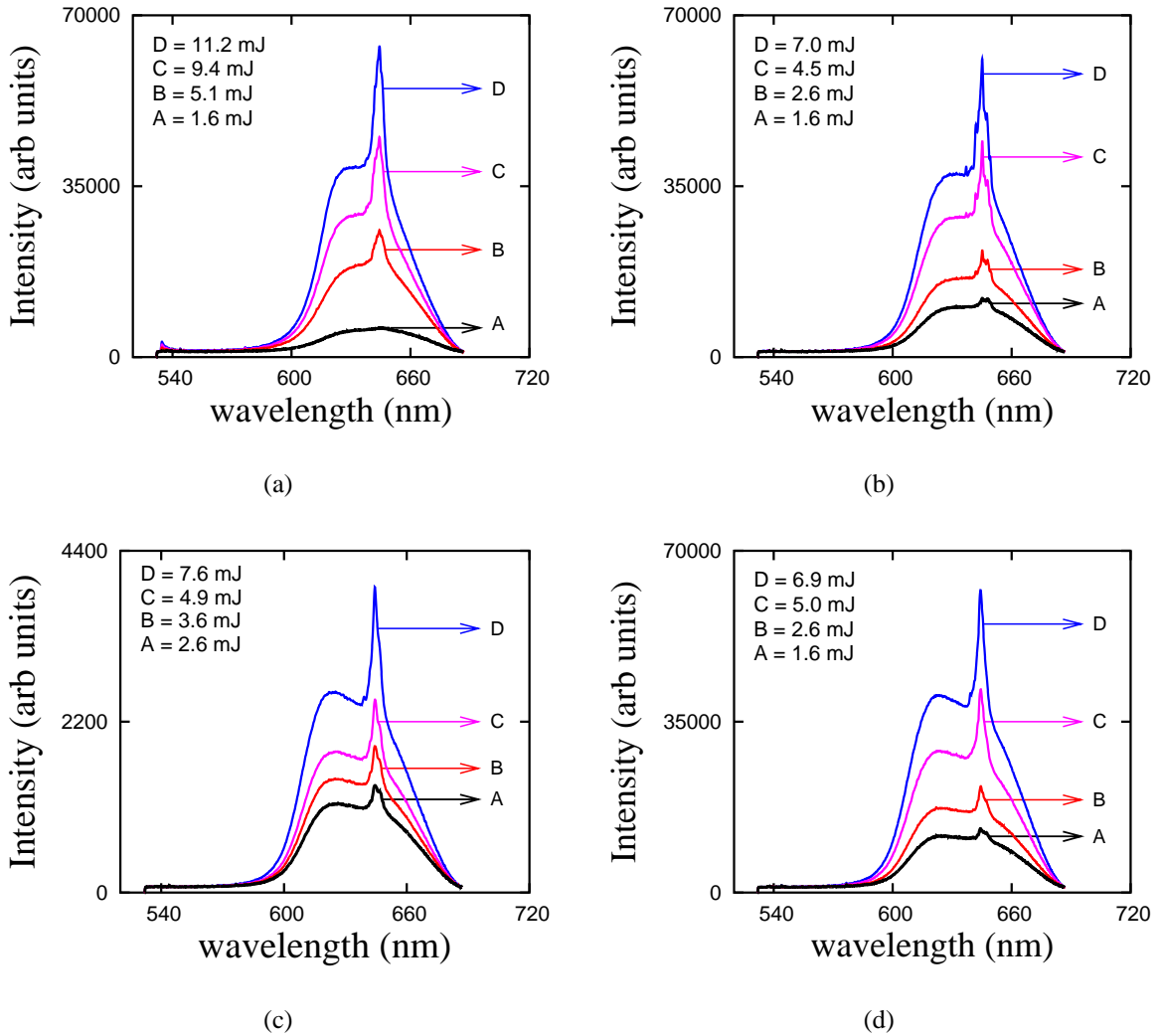
Figure 4.7: *Emission spectra as function of pump energy for N=500 F-RAM embedded in passive scattering medium : (a) polystyrene microspheres (size = 0.13 μm, density ~9.4 × 10^{13}/cc), (b) polystyrene microspheres (size = 0.13 μm, density ~9.4 × 10^{12}/cc), (c) polystyrene microspheres (size = 0.13 μm, density ~9.4 × 10^{11}/cc), (d) water.*
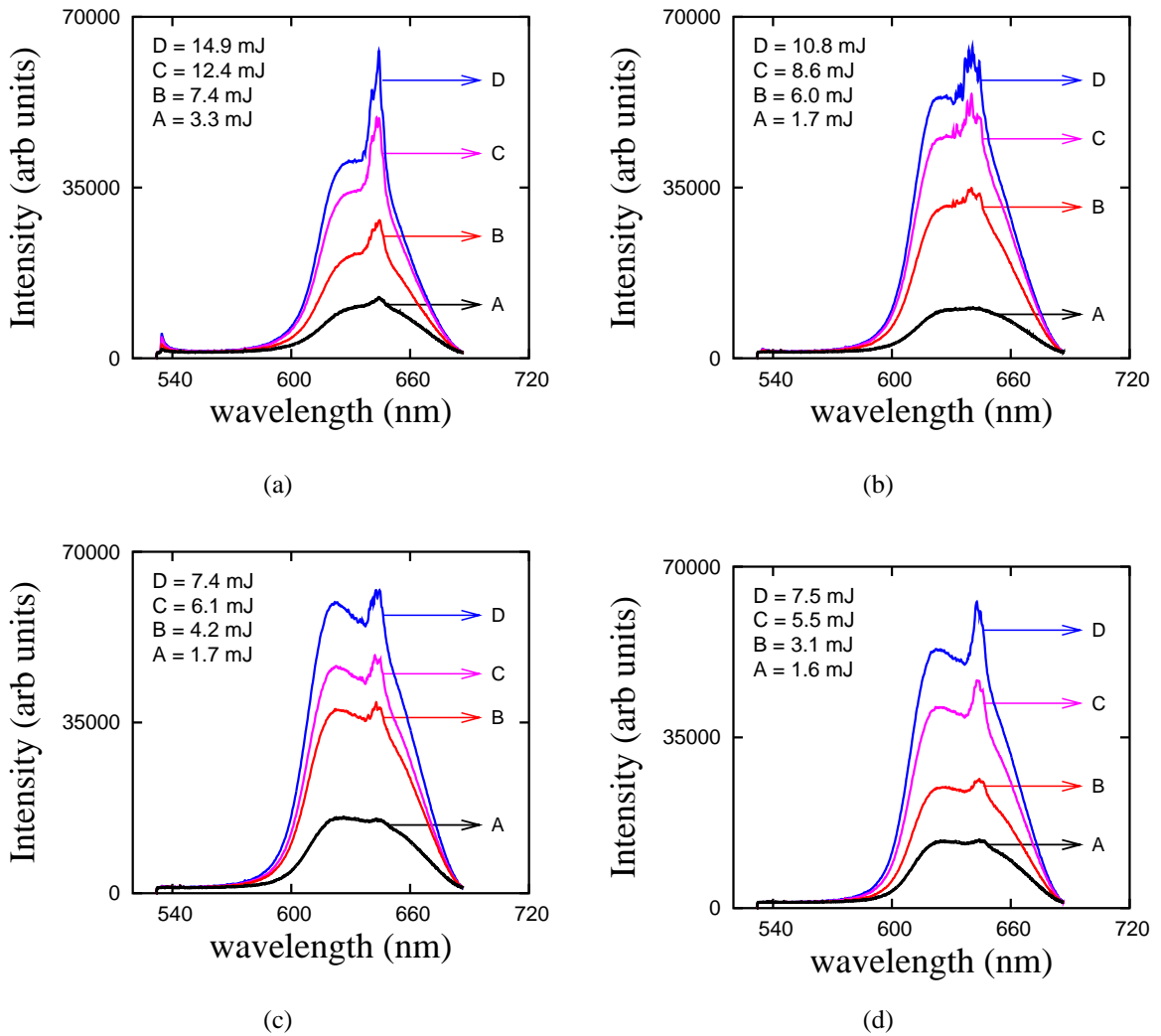
Figure 4.8: *Emission spectra as function of pump energy for millimeter (~2-3 mm) sized pieces of active fiber embedded in passive scattering medium : (a) polystyrene microspheres (size = 0.13 μm, density ~9.4 × 10^{13}/cc), (b) polystyrene microspheres (size = 0.13 μm, density ~9.4 × 10^{12}/cc), (c) polystyrene microspheres (size = 0.13 μm, density ~9.4 × 10^{11}/cc), (d) water.*

pump energy ($\sim$ 3 mJ) exhibit broad emission width $\sim$ 30-40 nm. On the other hand, the spectra (D) corresponding to pump energies $\sim$ (8-15) mJ exhibit relatively narrowed emission (with the intensity peaking at $\sim$ 640 nm).

On comparing the emission spectra in Figs 4.7 and 4.8, for a given passive scattering medium, we note that the narrowing of the emission spectra above a pump threshold (gain narrowing) is more pronounced in the N=500 F-RAM which contains long active fiber pieces, than that in the millimeter sized pieces of active fiber. This observation, clearly, shows that light amplification in the N=500 F-RAM is higher, due to the presence of long amplifying photon paths, than that in the millimeter sized pieces of active fiber.

Intensity histograms

As an F-RAM is a random aggregation of segments of active fiber, many configurations are possible for the same macroscopic composition of the F-RAM. Our experiment was aimed at studying the variation in emission intensity over these random configurations, and, therefore, the sample was stirred to change the configurations, and the corresponding spectra recorded. In this manner, spectra for nearly about 500 different configurations of the F-RAM were obtained. Here, we would like to point out that the collected intensity (I_o) contains the unamplified spontaneous emission (I_{spont}) too, which must be subtracted, so as to ensure analysis of only the stimulated emission from the system. We will, in the rest of the chapter, refer to this intensity as $I = I_o - I_{spont}$. Intensity histograms were then constructed, at a chosen wavelength, by plotting P(I), the number of times an intensity value was obtained (normalized to the total number of spectra), as a function of intensity, I. In particular, for each F-RAM, the intensity histograms were constructed for peak (λ_p) and off-peak (λ_{op}) wavelengths, where, λ_p refers to the wavelength at which the spectrum had an intensity maximum and λ_{op} to the wavelength well removed from the peak. Thus, λ_p and λ_{op} correspond to the maximum and the minimum gain respectively, in the system. Note that our samples are large enough to ensure spatial ergodicity.

To examine the effect of altering the gain by pumping, on the statistical fluctuations of emission intensity from F-RAM, we studied, the F-RAM consisting of N=500 active fiber

pieces (following the probability density $p(l)$, Eq 4.6), embedded randomly in passive scattering medium of granular starch, as function of pump energy. Figures 4.9(a-c) give the intensity values at $\lambda_p = 640$ nm as function of configuration for the N=500 F-RAM, at increasing pump energies of 3 mJ, 6 mJ and 12 mJ respectively. Figures 4.9(d-f) give the corresponding intensity histograms. It is readily seen that the configuration-to-configuration fluctuations are small at the sub-threshold pump energy of 3 mJ (Fig. 4.9(a)), and the corresponding statistics is nearly Gaussian (Fig. 4.9(d)). At a higher pump energy of 6 mJ (slightly above the lasing threshold), the intensity values show a few large jumps as the configuration is altered (Fig. 4.9(b)) that manifest themselves as a tail developing in the corresponding histogram (Fig. 4.9(e)). At a much higher pump energy (12 mJ), above the lasing threshold, the intensity values show many large jumps (Fig. 4.9(c)) with a pronounced Lévy-like tail in the histogram (Fig. 4.9(f)). A fit to the power law $p(g) \sim g^{-(1+\alpha)}$, gave exponents $\alpha = 1.77$ and 0.82 at pump energies of 6 mJ and 12 mJ, respectively, thereby demonstrating tunability of the Lévy exponent (with the smaller exponent indicating a fatter tail). It may be noted that, when the pumping is doubled (while keeping the other RAM parameters the same), the exponent is found to be halved (as expected from Eq 4.19).

We now discuss these experimental results in the light of our theoretical analysis (section 4.4), considering first the case of above-the-threshold pumping. As the sample contains a large number of short fibers, a photon typically traverses a large number of short steps as it is multiply scattered by the passive scatterers or is guided by very short active fiber pieces, resulting in configuration-to-configuration fluctuations in the emission intensity that are small and of nearly the same magnitude. Occasionally, however, a long segment of active fiber guides it over relatively large lengths and amplifies it considerably causing a sudden large jump in intensity (Fig. 4.9(c)). This is similar to a Lévy flight, and we may aptly term such an F-RAM a Lévy laser. At sub-threshold pumping, however, the gain is small, and the emission even from a long fiber is small, and hence the Gaussian statistics of the fluctuations (Fig. 4.9(d)).

At the off-peak wavelength ($\lambda_{op} = 685$ nm), the configuration-to-configuration fluctuations remained small (Figs 4.10(a-c)), and the histograms exhibited Gaussian statistics at all
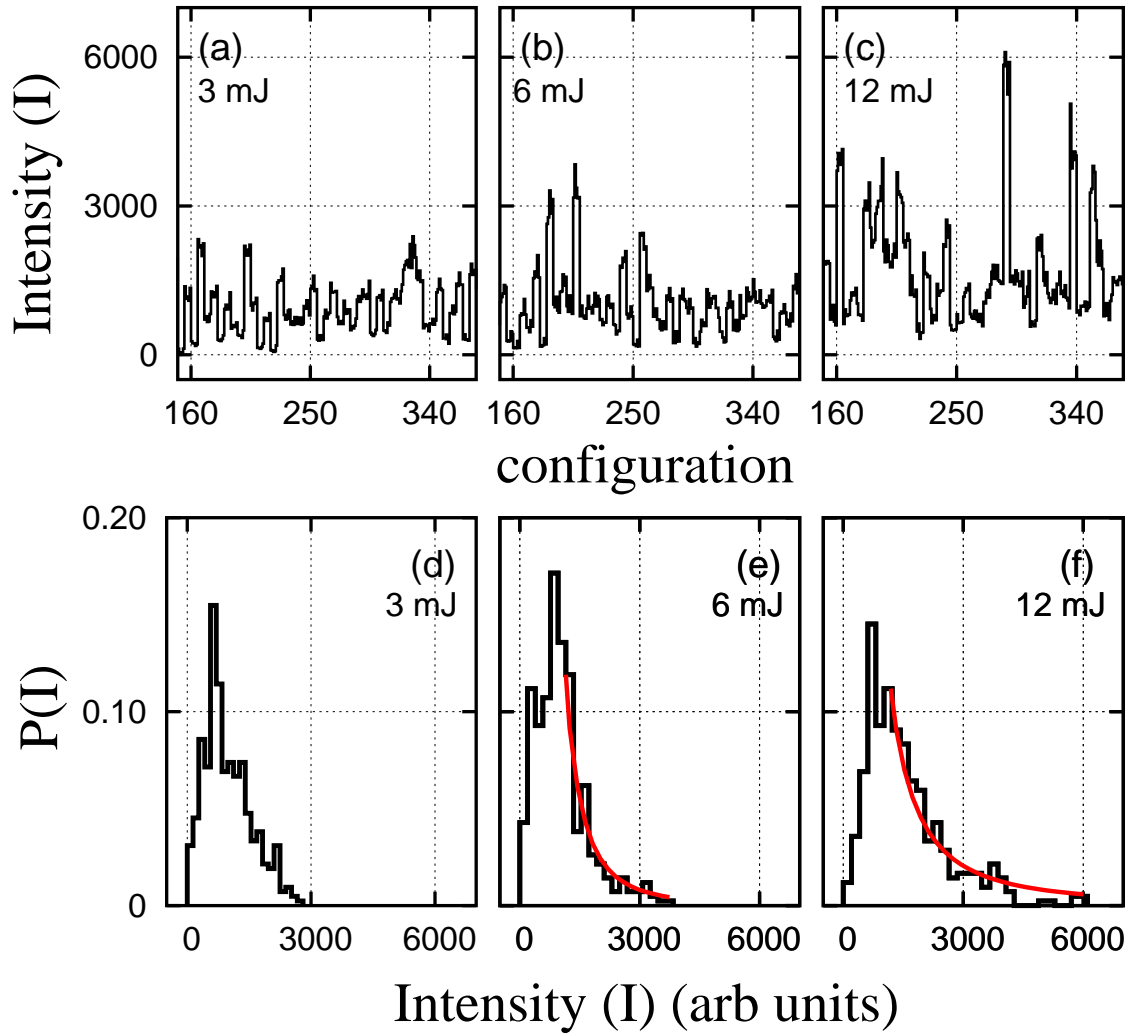
Figure 4.9: *N = 500 F-RAM embedded in passive scattering medium of granular starch (λ_p = 640 nm) : (a),(b) and (c), give the configuration-to-configuration fluctuation in the emission intensity; (d), (e) and (f), give the corresponding intensity histograms, at pump energies of 3, 6 and 12 mJ respectively. The power-law fits (red curves) to (e) and (f) with α = 1.77 and 0.82, respectively, are also shown.*

the three pump energies (Figs 4.10(d-f)). This observation can be attributed to low gain in the system at λ_{op}.

To verify that the presence of the exponentially rare long paths was crucial to the Lévy statistical fluctuations, we made a "powdered-F-RAM", that contained the same volume-fraction of the active medium as the N= 500 F-RAM, but with the active medium cryogeni-cally crushed to nearly uniform sub-millimeter sizes ($l_a \ll l_g$). The powdered F-RAM was, first, checked for gain-narrowing. Figures 4.11(a,b) show the emission spectra as a function of pump energy for the powdered F-RAM in water and polystyrene microspheres (size = 0.13 μm, density ~9.4×10^{12}/cc), respectively. Each figure contains five curves : (A-E) recorded at increasing pump energies. Curves (A) show the emission spectra at lowest pump energy (below the lasing threshold), which are quite broad and have FWHM of $\sim$ 40-50 nm. The emission spectra (B-D) clearly depict the onset of narrowing of spectral width to a few tens of nanometers. Emission spectra (E) at the highest pump energy (above the lasing threshold) has a FWHM of a few nanometers. Thus, these observations show that gain narrowing sets in the "powdered-F-RAM" as function of pump energy.

Now, the powdered active fiber was added to the same volume-fraction of passive gran-ular starch as in the N = 500 F-RAM. Thus, the sole distinction between the two systems was that while one (the N=500 F-RAM) contained exponentially rare long pieces of active fiber, the other (the powdered F-RAM) had only short pieces. Spectra for 420 configurations of the powdered-F-RAM were recorded, and the histogram for λ_p constructed. The statistics was clearly Gaussian (Fig. 4.12(b)). In contrast, Lévy statistics (α = 0.82) was obtained for the F-RAM at much lower pump energies (Fig. 4.12(a)), proving that it is the existence of the rare long paths that leads to the Lévy-like fat tail.

Similar crossover from the Gaussian to the Lévy statistics was observed in N = 350, 800 F-RAMs with passive scattering media of polystyrene microspheres, pieces of white optical fiber (non- amplifying, length $\sim$ 0.5 mm to 1 mm), glass pieces and sugar grains.
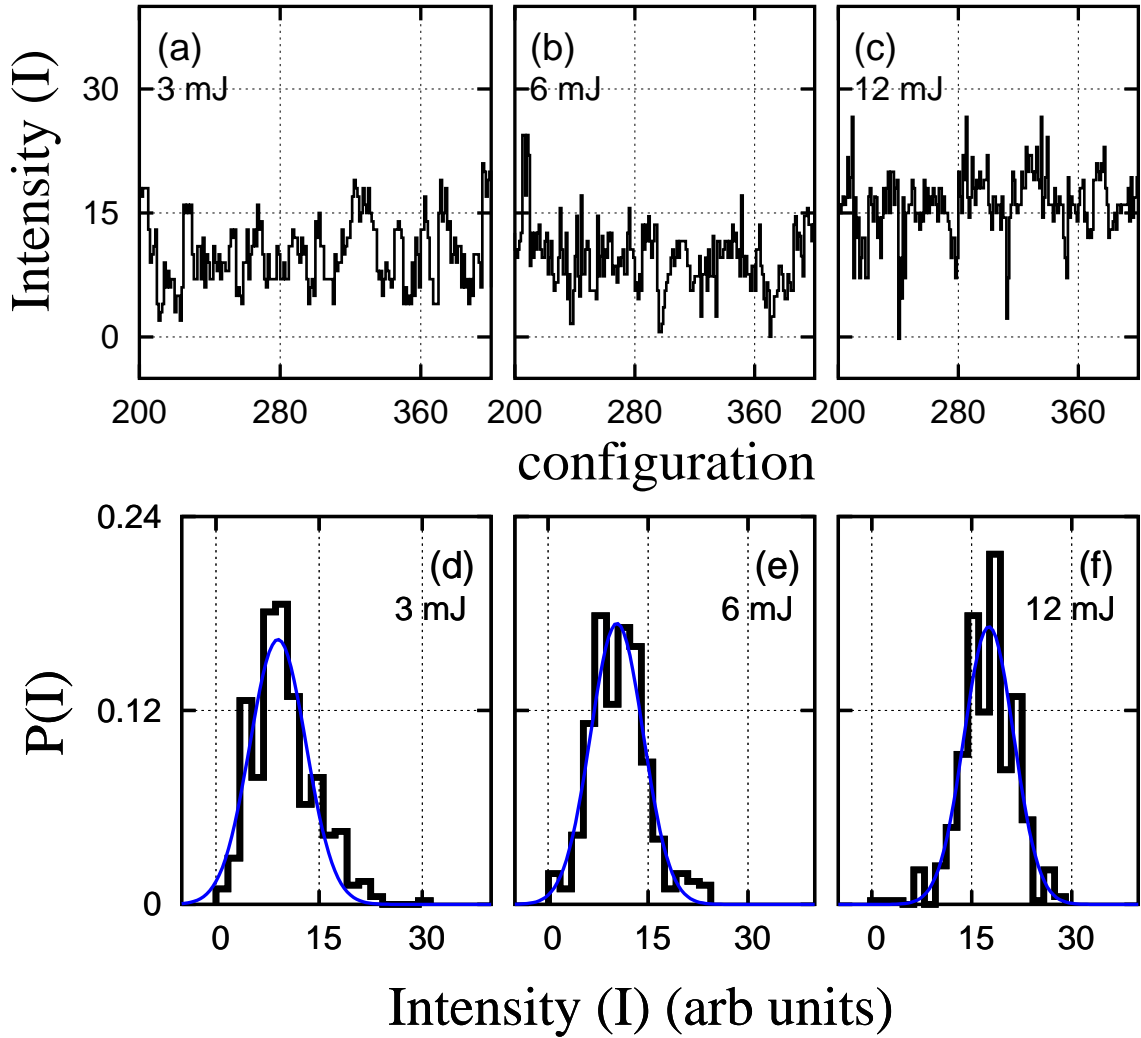
Figure 4.10: *N = 500 F-RAM embedded in passive scattering medium of granular starch, (λ_{op} = 685 nm). (a),(b) and (c), give the configuration-to-configuration fluctuation in the emission intensity; (d), (e) and (f), give the corresponding intensity histograms and their Gaussian fits (blue curves), at pump energies of 3, 6 and 12 mJ respectively.*
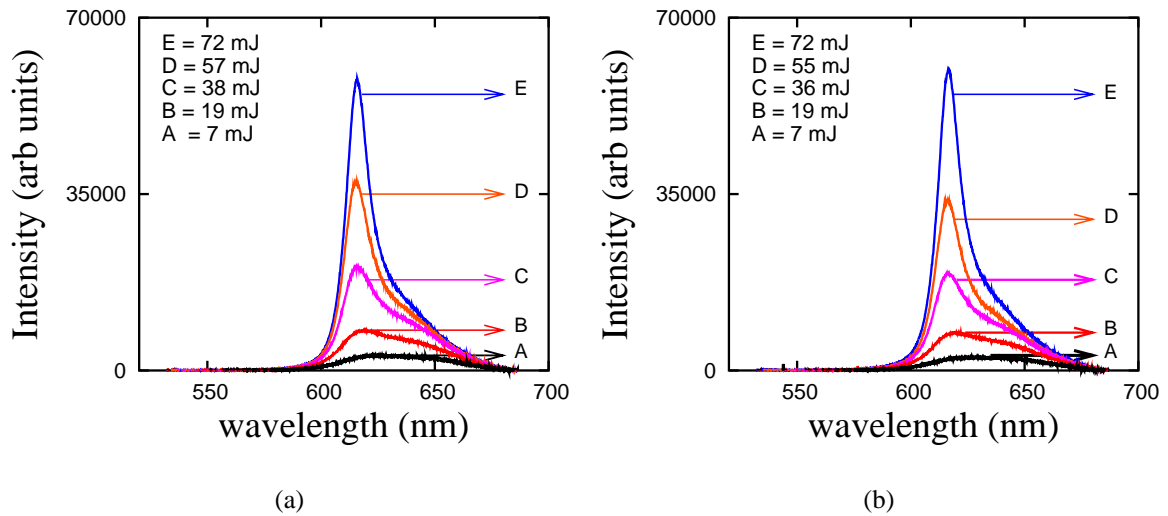
Figure 4.11: *Emission spectra as function of pump energy for powdered F-RAM embedded in passive scattering medium : (a) water, (b) polystyrene microspheres (size = 0.13 μm, density ∼9.4 × 10^{12}/cc).*

4.7   RAM vs F-RAM

The F-RAM is notably different from a conventional RAM in several aspects. As opposed to the RAM that has a bulk (three dimensional) active medium (optically pumped laser dye solution) with point-like (zero dimensional) scatterers randomly embedded in it, an F-RAM, has a passive, scattering bulk with active (one dimensional) fibers embedded randomly in it. Further, unlike the conventional RAM, during its traversal through the (passive) bulk medium, in an F-RAM, the photon does not get amplified. Consequently, a greater refractive index mismatch between the active (fiber) and the passive (bulk) media, which in the case of RAM leads to greater amplification due to increased path length in the bulk media, is likely to result under some conditions in just the opposite in an F-RAM, as it enhances scattering off the active fiber.
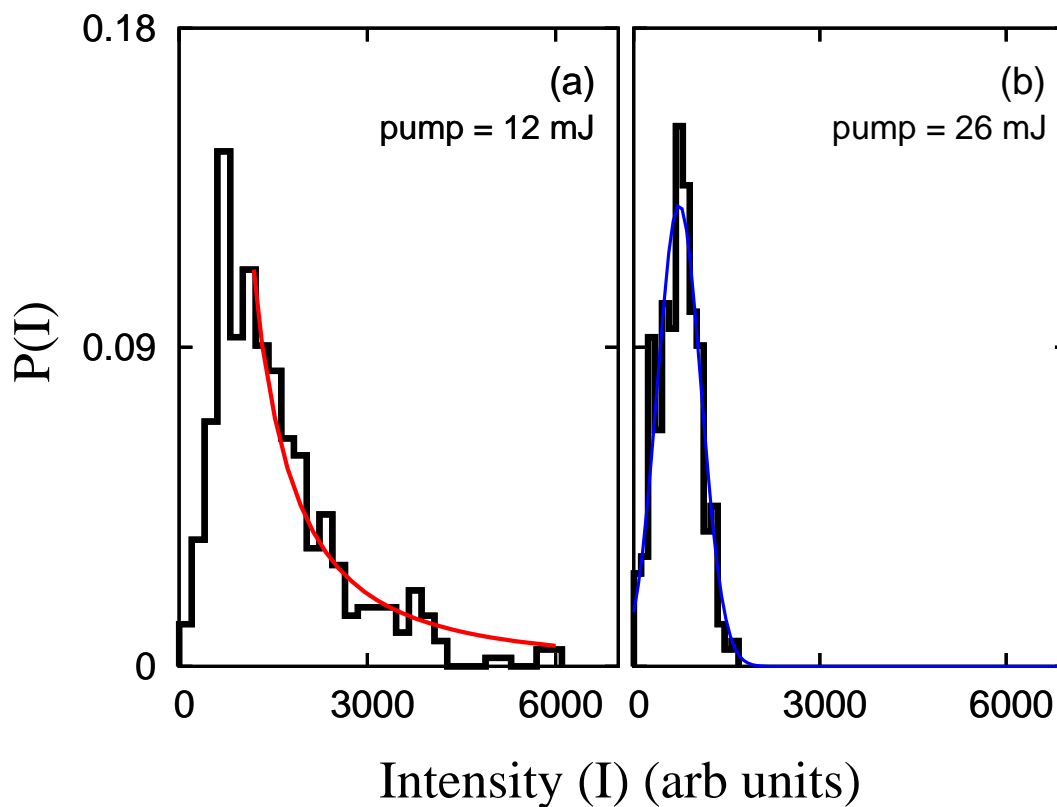
Figure 4.12: *Intensity histograms for (a) N=500 F-RAM embedded in passive scattering medium of granular starch at λ_p = 640 nm (b) powdered F-RAM at λ_p = 620 nm. Power-law fit (red curve) to (a), with α = 0.82 and the Gaussian fit (blue curve) to (b) are also shown.*

4.8   Conclusions

We made a novel specially structured model RAM, which we term an F-RAM (Fiber-Random Amplifying Medium), consisting of an aggregation of active fiber pieces embedded randomly in a passive scattering medium. The lengths of the active fiber pieces in the F-RAM, was tailored so as to have large number of short active fibers but exponentially small number of long active fibers. Thus, though the photon is exponentially amplified within a long active fiber, the probability for the photon to enter a long active fiber is exponentially small.

Thus, while our main emphasis in this work is on Lévy statistics with tunable exponent obtaining in the context of RAM, the addition of segments of fiber with the length typically much greater than the mean free path of the passive scattering medium in which they are embedded, simulates a Lévy flight. Such a system with exponentially rare occurrence of long flights provides an experimental realization of the Arrhenius cascade in optics.

Our theoretical analysis of the statistical fluctuations in emission intensity from the F-RAM, predicted a crossover from the Gaussian to the Lévy statistics as function of various parameters characterizing the F-RAM (e.g., pumping/gain). Further, we performed a detailed experimental study of the fluctuations in the emission intensity from the F-RAM, by varying the number of active fiber pieces, passive scattering media and the pump energy. These experiments (as suggested by our theoretical analysis) demonstrated a crossover from the Gaussian to the Lévy statistics with tunable Lévy exponent, as a function of pump energy. We show that the Lévy statistics in F-RAM is attributable to the "long but rare" amplifying paths traversed by the photons in the active fibers. Most of the active fibers in the F-RAM are short, the associated light amplification is less, resulting in low emission intensities. However, in the exponentially rare event of a photon entering a long active fiber it undergoes exponential amplification resulting in very high intensity. This results in large fluctuations in the emission intensity exhibiting Lévy statistics and hence we term it a Lévy laser.

Bibliography

[1] F. Bardou, arXiv:physics/ 0012049 v1, 20 Dec 2000.

[2] C. Kittel, "Free electron fermi gas," in *Introduction to solid state physics*, (John Wiley and Sons, Asia, 1996) pp. 141-172.